

Experimental and Numerical Studies on Development of Fracture Process Zone (FPZ) in Rocks under Cyclic and Static Loadings

M. Ghamgosar¹ · N. Erarslan^{1,2}

Received: 4 January 2015 / Accepted: 21 June 2015 / Published online: 1 July 2015
© Springer-Verlag Wien 2015

Abstract The development of fracture process zones (FPZ) in the Cracked Chevron Notched Brazilian Disc (CCNBD) monsonite and Brisbane tuff specimens was investigated to evaluate the mechanical behaviour of brittle rocks under static and various cyclic loadings. An FPZ is a region that involves different types of damage around the pre-existing and/or stress-induced crack tips in engineering materials. This highly damaged area includes micro- and meso-cracks, which emerge prior to the main fracture growth or extension and ultimately coalescence to macrofractures, leading to the failure. The experiments and numerical simulations were designed for this study to investigate the following features of FPZ in rocks: (1) ligament connections and (2) microcracking and its coalescence in FPZ. A Computed Tomography (CT) scan technique was also used to investigate the FPZ behaviour in selected rock specimens. The CT scan results showed that the fracturing velocity is entirely dependent on the appropriate amount of fracture energy absorbed in rock specimens due to the change of frequency and amplitudes of the dynamic loading. Extended Finite Element Method (XFEM) was used to compute the displacements, tensile stress distribution and plastic energy dissipation around the propagating crack tip in FPZ. One of the most important observations, the shape of FPZ and its extension around the crack tip, was made using numerical and experimental results, which supported the CT scan results. When the

static rupture and the cyclic rupture were compared, the main differences are twofold: (1) the number of fragments produced is much greater under cyclic loading than under static loading, and (2) intergranular cracks are formed due to particle breakage under cyclic loading compared with smooth and bright cracks along cleavage planes under static loading.

Keywords FPZ · Subcritical crack propagation · Rock fracture toughness · CCNBD · CT scan · SEM

1 Introduction

Linear elastic fracture mechanics (LEFM) is applicable for brittle materials that behave elastically until fracturing takes place. In that case, energy stored in material during loading is converted to elastic strain energy and surface energy due to the formation of the main crack (Spyropoulos et al. 1999; Griffith 1920). However, rocks are not entirely brittle and exhibit pre-peak nonlinearity and post-peak unloading called ‘strain-softening’ (Labuz et al. 1987; Franklin et al. 1988). Two physical phenomena are considered when determining the applicability of LEFM: (1) development of microcracks near the pre-existing crack tip and (2) ligament connection or crack bridging across the main crack due to aggregate interlock, unbroken fibre, and so on. In addition, LEFM assumes that the material is homogeneous, whereas rocks would be considered homogeneous only at a scale much larger than the grain size. Therefore, the applicability of LEFM depends on the size of the specimen considered and the pre-existing cracks in rocks (Mindess 1984).

Crack initiation, propagation and specimen failure do not occur at the same time; rather, each separately forms a

✉ M. Ghamgosar
m.ghamgosar@uq.edu.au

¹ The University of Queensland, School of Civil Engineering, St Lucia, Brisbane, QLD 4072, Australia

² Adana Science and Technology University, Mining and Mineral Processing Engineering, Adana, Turkey

particular fracture process. However, the crack initiation from a pre-existing crack tip, called the primary crack, does not have to lead to failure, since this initial crack propagation may be arrested at some stress level. It is suggested that the crack propagation in rocks, concrete and other brittle materials is associated with the formation of microcracks at the crack tip, and interlocking of particles behind the crack tip (also called ligament connection or crack bridging). These phenomena are different from the plastic yielding near the crack tip in metals (Tang and Yang 2012). With increasing load, secondary cracks develop and propagate until they reach the boundary, leading to final failure, or until they act as a ligament between primary cracks to cause a final failure plane (Wang et al. 2004). Horii and Nemat-Nasser (1986) investigated the micromechanics of axial splitting and faulting using certain mathematical models to analyse these failure modes, new simple closed-form analytic solutions of crack growth in compression and experimental results. These authors proposed a simple two-dimensional mathematical model for the analysis of the brittle–ductile transition process and a closed-form analytical solution to compare the results with those of proposed mathematical models (Horii and Nemat-Nasser 1986).

The tensile fracture of a brittle solid is relatively simple and well understood; a single flaw propagates unstably when the stress intensity, K , at its tip exceeds the critical stress intensity (or fracture toughness) K_C , of the solid. The cracks then grow in a stable way until they start to interact; interaction increases the stress intensity driving crack growth and leads to instability and final failure (Eberhardt et al. 1998).

The mode I (tensile) stress intensity factor K_I itself is dependent on the crack length, C , the applied stress, σ_A , and a geometry factor, ψ (Anderson 2005).

$$K_I = \psi \sigma_A \sqrt{\pi C} \quad (1)$$

Classical fracture mechanics suggests that the fracture initiation from the fracture tip takes place when

$$K_I = K_{IC} \quad (2)$$

where K_I is mode I (tensile) stress intensity factor and K_{IC} is the mode I fracture toughness, a material constant that can be determined by laboratory tests (Anderson 2005). The subcritical crack growth theory states that slow crack extension takes place when:

$$K_I < K_{IC} \quad (3)$$

When a subcritical crack (a crack whose stress intensity factor is below the critical value) is subjected to either repeated or fatigue load, or is subjected to a corrosive environment, crack propagation will occur. Subcritical crack growth is one of the main explanations for creep

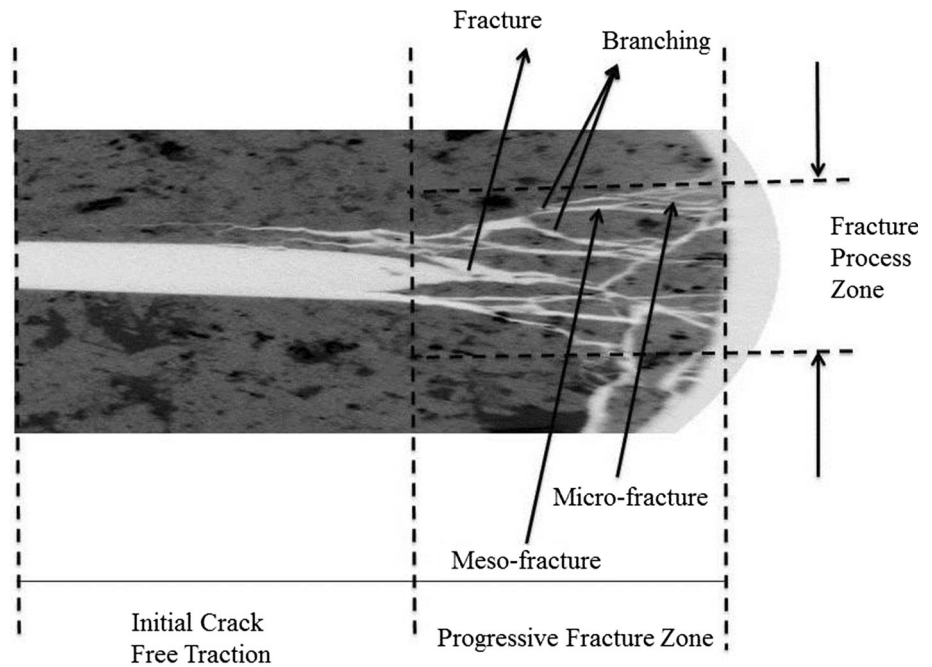
damage mechanism in rocks. In some fatigue research, damage accumulation in brittle materials under cyclic loading has been explained by the ‘creep’ mechanism and ‘stress corrosion’ (Evans 1972). Evans (1974) analysed the failure of materials due to slow crack growth, under dynamic loading conditions in terms of crack velocity and stress intensity relationships. Evans and Fuller (1974) showed that this type of analysis can fully describe the failure characteristics for both constant strain rate and constant stress rate loading. The analysis is used to predict the variations of strength and subcritical crack growth with strain rate and stress rate. One of the most fundamental parameters in fracture mechanics is critical fracture toughness (K_{IC}), which describes the resistance of a material to crack propagation. K_{IC} is an important material property, which corresponds to the critical state of the stress intensity factor required for crack initiation and subsequent propagation. In geomaterial like concrete and rocks, the region near the crack tip containing the microcracked zone and ligament connections is called fracture process zone (FPZ) (Fig. 1).

The effect of FPZ on propagation of a tensile crack has been a subject of considerable interest over the years, and is the subject of this research (Tang and Yang 2012; Labuz et al. 1987). The size of an FPZ may depend on the grain size of rocks (Maji and Wang 1992). Maji and Wang (1992) also suggested that the ligament connection is the main feature in FPZ that causes crack bridging to happen there. Several researchers have modelled the dimensions of FPZ and its physical characteristics based on the nonlinear dynamics and behaviour of rocks. Details of various experimental studies have been summarised by Ouchterlony (1980). Schmidt and Lutz (1979) suggested that the crack length ‘ a ’ should be larger than $2.5 \times (K_{IC}/\sigma_t)^2$, where K_{IC} is the critical stress intensity factor (SIF) and t is the tensile strength of the rock. In addition, they suggested a maximum normal stress criterion to describe the shape of the crack tip FPZ in rock. This criterion is based on the assumption that the formation of FPZ takes place because of excessive tensile stress [i.e. when the local maximum principal stress near the crack tip reaches the ultimate uniaxial tensile strength (t) of the rock].

The description of FPZ in rocks is more difficult than in metals due to the complexity of the fracturing process in rock. From the method for determining the principal stresses in front of the crack tip in the elastic region, the principal stresses in the vicinity of a crack tip in plastic zone can be obtained as follows (Whittaker 1992):

$$\begin{bmatrix} \sigma_1 \\ \sigma_2 \end{bmatrix} = \frac{K_I}{\sqrt{2\pi r}} \cos \frac{\theta}{2} \begin{bmatrix} 1 + \left| \sin \frac{\theta}{2} \right| \\ 1 - \left| \sin \frac{\theta}{2} \right| \end{bmatrix} \quad (4)$$

Fig. 1 Developed FPZ and its components in a CCNBD specimen



Making a substitution of maximum principal tensile stress σ_1 given by Eq. 4 into when $\sigma_1 = \sigma_t$ yields the shape of FPZ as follows (Whittaker 1992):

$$r(\theta) = \frac{1}{2\pi} \left(\frac{K_I}{\sigma_t} \right)^2 \cos^2 \frac{\theta}{2} \left(1 + \left| \sin \frac{\theta}{2} \right| \right)^2 \quad (5)$$

Since many criteria do not account for the stress redistribution outside FPZ, the actual size of the FPZ in rocks should be larger. It is assumed in the literature that the macro crack is composed of the traction-free length behind the crack tip plus the FPZ (Whittaker 1992). Closing forces in this zone represent the resistance of the material not yet ruptured or in contact, and are a function of crack opening forces. Thus, unbroken/interlocked ligaments are prevalent behind the crack tip, indicating that the crack must open further to overcome the closing forces. Physically, this region may be caused by the variation in local stress between grains and pre-existing microcracks, so differentiating between the two zones may be obscure (Labuz et al. 1987). In this paper, different extensions of micro-fractures in FPZ region were examined by performing the CCNBD test and simulated numerically by XEFM analysis.

2 Experimental Study

2.1 Mode I (Tensile) Fracturing Tests

The Cracked Chevron Notched Brazilian Disc (CCNBD) samples were used in both static and cyclic loadings to

determine the mode I fracturing value of the selected rock types. The CCNBD specimens were preferred in the entire test series rather than using short rod (SR) specimens. As far as a general comparison between the two methods is concerned, the CCNBD method definitely had advantages in terms of simplicity of sample preparation and less material required for testing. It is also unnecessary to perform pre-cracking for a CCNBD specimen because it uses a chevron notch that self-pre-cracks during testing and leads to stable crack propagation. Another remarkable advantage of the CCNBD method over the SR method in terms of accuracy is higher load capacity and consistent results for each test. In this research, all the CCNBD samples show high accuracy in maximum load measurements. In addition, it is possible to measure mode I (tensile), mode II (shear) and mixed-mode I–II (tensile and shear) fracture toughness by inclining the notch at different angles with respect to the axis of diametral load. Moreover, it is believed that obtaining the FPZ zone with CCNBD geometry is more precise than obtaining with SR specimen geometry, as CCNBD has an embedded chevron notch crack whereas SR has edge notch crack. The other significant and fundamental laboratory experiments used in this research include: Uniaxial Compressive Strength test (UCS), Brazilian Indirect Tensile Test (BTS), fracture toughness test using the CCNBD and the Computed Tomography (CT) scan that uses X-rays and digital computer technology to create cross-section images of the damaged rock specimens. A series of BTS specimens were tested to evaluate the effect of cyclic loading on the tensile strength of two brittle rock types' monsonite and tuff.

Further, the CCNBD test was carried out to determine the mode I fracture toughness of rocks (Fig. 2).

The CCNBD test has advantages over other International society for rock mechanics (ISRM) or American society for testing and materials (ASTM) methods in terms of the simplicity of sample preparation and the reduced material required for testing (Erarslan and Williams 2012). A fully digital cutting machine with a circular 40 mm diamond saw was used to prepare the notched cracks, according to the ISRM suggestions (Fig. 3a). Prepared tuff and monzonite CCNBD specimens are shown in Fig. 3b, c, respectively. All geometrical dimensions were selected according to the specifications recommended by ISRM (Fowell et al. 1995). To achieve valid results, there are two important dimensions, that is, notched crack length α_1 and the ratio of specimen thickness to diameter α_B that must fall within the ranges outlined in ISRM suggested method (Fowell et al. 1995). In this study, the thickness of monzonite disc-shaped samples was $B = 22.3$ mm, inner chevron crack notch half length, $\alpha_0 = 5.8$ mm, and outer chevron notched crack half length, $\alpha_1 = 15.6$ mm (Fig. 3c). The diameter of the CCNBD for tuff specimens was different from the monzonite samples because of greater core diameters. Geometrical dimensions of tuff specimen were $B = 25$ mm, $\alpha_0 = 8$ mm and $\alpha_1 = 18$ mm. All selected dimensions for the geometry of specimens in this study were valid based on the ISRM suggested method. Some of the prepared CCNBD specimens are shown in Fig. 3b, c.

An Instron loading machine with a capacity of ± 150 kN ($\pm 25,000$ kgf, $\pm 56,000$ lbf) was used for static and cyclic loading tests. An Instron 2670–132 series crack opening displacement (COD) gauge was used to measure the crack mouth displacement, in which the optimum length of travel was 4 mm (Fig. 3d). The length of COD gauge was 10 mm, which is set up and mounted in CCNBD specimen according to the British Standard BS 5447 and American standard ASTM 399 70T. The disc specimens were diametrically loaded parallel to the diametral compressive loading directions with a notch crack inclination angle of zero ($\beta = 0^\circ$) to provide a mode I fracture condition. The applied load, diametral displacement, and crack mouth displacement were continually recorded during the tests using a computerised data logger. Static tests were performed following the ISRM instructions (Fowell and Xu 1994; Fowell et al. 1995).

2.2 X-Ray Computed Tomography Scanning Tests

3-D X-ray micro-focus CT scanning techniques were used in this study to investigate and quantify the physical properties of the damaged zone, such as crack porosity (cracked volume/total volume) and crack density (number of cracks per mm^3). Some samples tested under both static and cyclic loading have been prepared for this test (Fig. 4). These samples were tested at the University of Queensland, Julius Kruttschnitt Mineral Research Centre (JKMRC). The X-ray detector is a high-resolution digital

Fig. 2 Configuration of the CCNBD sample according to the ISRM suggestions

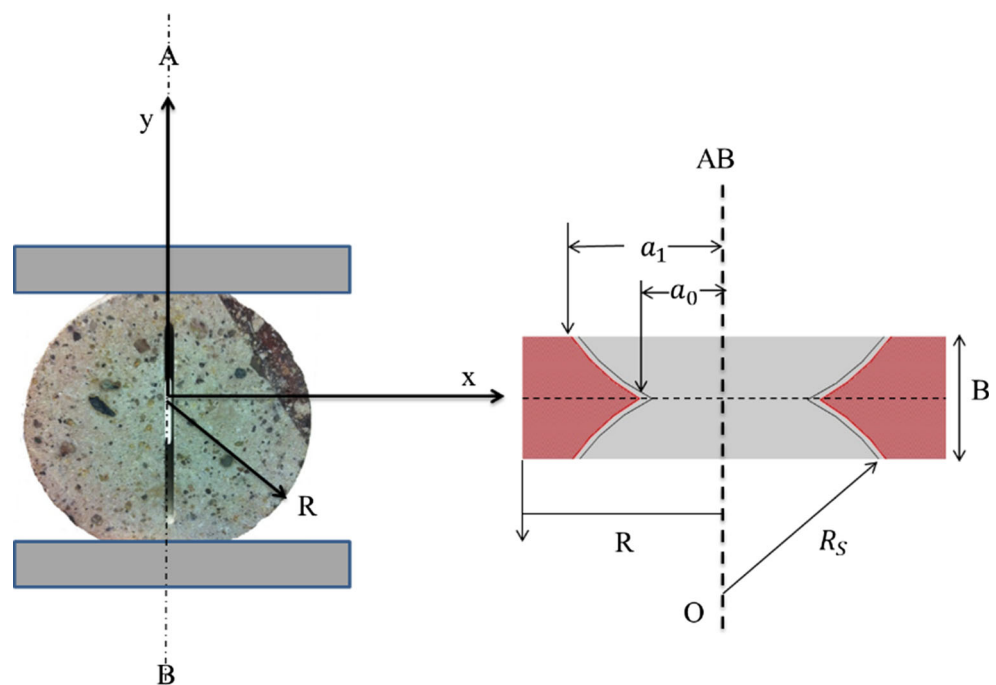




Fig. 3 CCNBD specimen preparation and experimental setup of CCNBD test according to ISRM suggestions

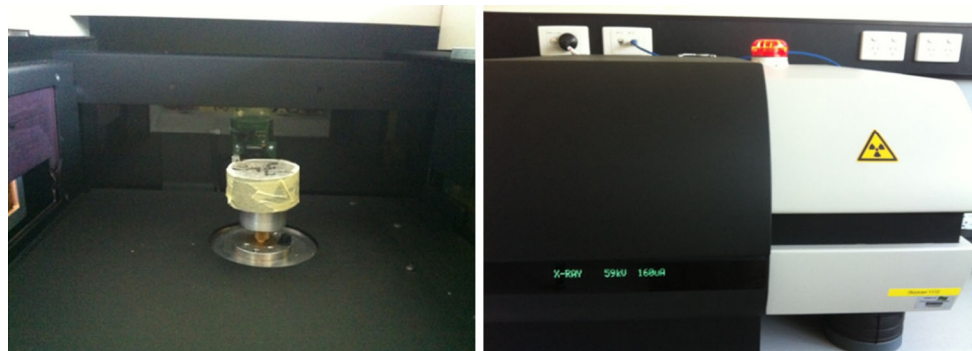


Fig. 4 Experimental setup for the X-ray analysis and a damaged rock sample after a fracture toughness test

X-ray camera detector system. This detector accumulates all the energy of the transmitted photons and provides the numerical data to be used in reconstructing an image. For each head, 1500 views of the sub-sample were taken over 360° rotation. Each sample was placed vertically within the scanner so that the X-ray intersected the sample perpendicular to the longitudinal axis. Once the scans were finished, the collected raw data (the series of rotational X-ray images) were reconstructed with an ultra-high-resolution noise reducing filtered back projection. For the SkyScan 1172, the X-ray micro-focus tube with $8 \mu\text{m}$ focal spot operates at 20–80 kV and $100 \mu\text{A}$ current while the source working at 20–100 kV and 0–250 μA has a $5 \mu\text{m}$ spot size. The special X-ray Charge-Coupled Device (CCD) camera is based on a 4000×2300 (10 Mp), or

1280×1024 (1.3 Mp) cooled CCD sensor with fibre optic coupling to the X-ray scintillator. For the 10Mp camera, the X-ray shadow projections are digitized as 1000×575 – 8000×2300 pixels with 4096 brightness gradations (12 bit). The reconstructed cross sections have a 1000×1000 – 8000×8000 pixels (floating point) format. The pixel size is isotropic and continuously variable from 0.9 to $35 \mu\text{m}$. Figure 4 represents the experimental setup for the CT scan test and a rock sample after a fracture toughness test.

To assess the micro-fracture patterns created under cyclic loading, the first series of CCNBD samples were tested with the CT scan technique. The second series of CT scan tests were performed for partially loaded specimens of 10, 50 and 80 % of ultimate tensile

strength (UTS) to compare the effect of different amplitudes in the development of the FPZ under cyclic loading.

3 Numerical Analyses

The extended finite element method (XFEM) was used in this research to perform the numerical simulations and related analyses. When the traditional finite element method (FEM) is used for a crack propagation modelling, any crack propagation starts from the edge of the elements whereas a numerical modelling is done based on the enrichment elements of FEM with XFEM with the help of additional degree of freedom (DOF) (Giner et al. 2009). Another advantage of the XFEM method is its independence to model mesh and the way it can be successfully applied to model the dynamic fracture propagation (Giner et al. 2009). The main parameters for the numerical analyses were the strain rate decomposition or cracking strain rate, the elasticity properties, a set of cracking condition and the evolution law for crack propagation in the FPZ simulations. One of the powerful models, which are utilised to analyse the brittle cracking, is the inelastic constitutive model used for modelling the fracturing process of Mode I fracturing simulations. All input parameters used in numerical models were obtained with the experiments and, ultimately, the brittle crack model was adopted for the stress-displacement analysis.

4 Results

4.1 Mode I Fracture Toughness Under Static Loading

Failure load and fracture toughness values of the Brisbane tuff and Cadia Valley monsonite specimens were determined with the CCNBD method. The maximum recorded load and the calculated fracture toughness values obtained from ISRM standard test CCNBD are shown in Table 1.

It is apparent from Table 1 that the average failure load for the tuff specimens is 4.67kN, almost half of the average failure load of monsonite specimens. The average fracture toughness magnitudes for monsonite and tuff specimens were measured at 1.29 and 2.09 MPa \sqrt{m} , respectively.

4.2 Mode I Fracture Toughness Under Cyclic Loading

Two types of cyclic loading were performed in this research using Instron WaveMatrix software. In the first type, which is called the ‘stepped’ type increasing cyclic

Table 1 Mode I fracture toughness values of Brisbane tuff, and Cadia Valley monsonite specimens obtained with CCNBD tests

Rock type	P_{max} (kN)	K_{IC} (MPa \sqrt{m})
Brisbane tuff-1	4.32	1.20
Brisbane tuff-2	4.26	1.18
Brisbane tuff-3	5.23	1.45
Brisbane tuff-4	4.19	1.16
Brisbane tuff-5	5.36	1.49
Average	4.67	1.29
Monsonite-1	8.36	2.32
Monsonite-2	7.21	2.00
Monsonite-3	7.06	1.96
Monsonite-4	7.64	2.12
Monsonite-5	6.91	1.91
Average	7.44	2.06

loading, the mean levels of each cyclic increase with constant frequencies ranged from 1 to 5HZ. In this model, cyclic waveforms start at the initial set point (starting value of the controlling channel at the beginning of a step), proceed to a peak amplitude (+ or -), reverse to the opposite peak amplitude, and then return to the initial set point. However, in the second type, called ‘continuous’ increasing cyclic loading, cyclic waveforms start at the initial set point, proceed to a peak and reverse to the end of last set point of the previous step. The fracture toughness results of both types cyclic loading are given in Table 2.

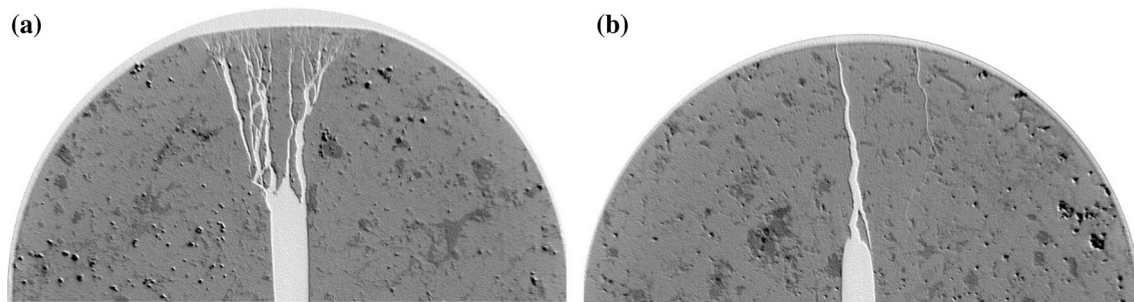
The fracture toughness value of Brisbane tuff specimens was 2.06 MPa \sqrt{m} with continuous type cyclic loading. This result shows a kind of ‘strain hardening’ behaviour in rock specimen whereas a serious fracture toughness reduction was obtained with the stepped type cyclic loading. On the other hand, fracture toughness values of monsonite specimens were decreased with both types of cyclic loading. This result is definitely worth further investigating the response of various rock types to dynamic and cyclic loadings. It was obtained from the stress-strain plots of stepped cyclic loading. The stiffness reduction occurs due to the emerging new micro-fractures in samples during unloading cycles. Another possible explanation for this strength reduction with stepped cyclic loading would be that the strain energy dissipation rate with the stepped cyclic loading may be greater than the strain energy dissipation rate with the continuous cyclic loading.

4.3 Computed Tomography Scan Test Results

The CT scan technique was used to quantify the FPZ under different cyclic loadings. As discussed earlier, nucleation of micro-fractures is the main reason for fracturing leading to failure in brittle rocks. The CT scan tool provides a clear

Table 2 Mode I fracture toughness values of Brisbane tuff and monsonite specimens obtained from CCNBD cyclic loading tests

Rock type	Continuous cyclic loading		Stepped cyclic loading	
	P_{\max} (kN)	K_{IC} (MPa \sqrt{m})	P_{\max} (kN)	K_{IC} (MPa \sqrt{m})
Brisbane tuff-1	3.67	1.02	2.59	0.72
Brisbane tuff-2	3.83	1.06	3.41	0.94
Brisbane tuff-3	4.55	1.26	3.66	1.01
Brisbane tuff-4	3.35	0.93	2.93	0.81
Brisbane tuff-5	4.82	1.34	4.29	1.19
Average	7.43	2.06	3.38	0.77
Monsonite-1	5.02	1.39	4.31	1.20
Monsonite-2	4.04	1.12	3.71	1.03
Monsonite-3	4.31	1.19	3.70	1.03
Monsonite-4	5.35	1.48	4.81	1.33
Monsonite-5	4.35	1.21	3.77	1.04
Average	4.61	1.28	4.06	1.13

**Fig. 5** CT scan images of CCNBD specimens with FPZ developed under, **a** cyclic and **b** static loading

monitoring of microcracks initiation and propagation in and around the FPZ. Dislocation of micro-fractures takes place in different ways with different rock types. In general, breaking the bonds between minerals and rock forming matrix happens due to two reasons: (1) concentration of stress at the tip of fractures and (2) formation of transcrytalline and inter-crystalline cracks (Gross and Seelig 2011). All those dislocations occurred because of the micro-fractures, such as intergranular and intragranular cracks caused by the inelastic behaviour of rocks (Fig. 5). The obvious difference between the fracturing of specimens tested under static loading and cyclic loading can be seen in Fig. 5. Some symmetrical fracture surfaces were seen in failed specimens tested under static loading whereas excessive small particles and arbitrary fracturing were observed in failed specimens tested under cyclic loading (Fig. 5). This mechanical behaviour shows that decohesion and loosening start with the development of FPZ in front of the notched crack under the cyclic loading. Similar results were obtained with the stepped cyclic loading, but not with the continuous cyclic loading. Moreover, CT scan results performed on the monsonite and tuff samples tested under static loading showed the micro-fractures initiated at the tip of notch crack as sharp cleavage cracks.

Further CT scans on CCNBD specimens showed the self-orientated stress-induced micro-fractures and their interactions caused subcritical cracks and enhanced energy dissipation. Static tests revealed the main crack propagation associated with the very small damage zone started from the tip of the notch crack and ended at the CCNBD circumference without any fracture branches. That is why any subcritical crack propagation before the final failure would not be expected. However, a great number of smooth and smaller cracks occurred in and around the FPZ, which leads to the formation of subcritical cracks under both types of cyclic loading. Those interesting and impressive results were studied further using XFEM analysis to evaluate the role of different stress components at the tip of notch cracks causing those cracks and branching. XFEM results are given in the following sections. It has been concluded that the width of FPZ can be defined by the determination of accumulated fracture branches depending on the type of cyclic loading (i.e. with various amplitude and frequency values). It was observed in this study that the size of FPZ was found to be extended by increasing the amplitude from 1 per cent UTS to 10 per cent UTS due to the increasing number of stress-induced subcritical cracks and micro-fractures around the tip of pre-existing cracks.

According to the CT scan analysis, the development and expansion of FPZ were found to be strongly dependent on the cyclic loading characteristics and specific parameters, such as type of mean stress value, amplitude and frequency. Thus, different types of cyclic loading tests have been conducted to explain this concept using CT scan observations on the failure surface of tested specimens without any surface preparation. Figure 6 shows a close look at the FPZ and crack branches developed in rock matrix under the stepped cyclic loading with increasing amplitude from 10 per cent UTS to 50 per cent and 80 per cent UTS.

In general, it was clearly seen that the number of microfractures and width of the FPZ increased with a rise in the amplitude from 10 per cent UTS to 50 % UTS and ultimately to 80 % UTS. Moreover, the shape of FPZ was found to be dependent on the material properties and other environmental conditions, such as structure of rock matrix pore pressure and thermal state. For instance, the fracture toughness value of monsonite specimens was found to decrease with the increasing temperature (Ghamgosar et al. 2014a).

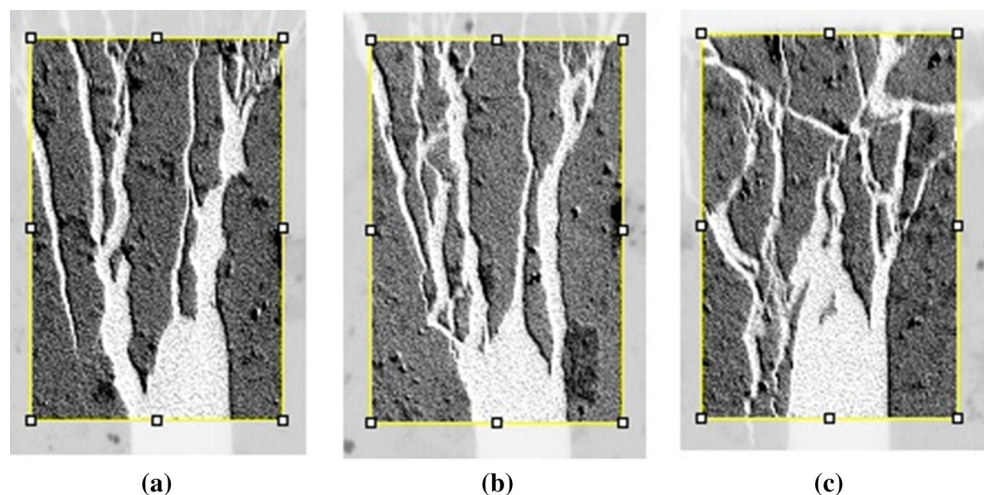
4.4 Results of Numerical Simulations

In LEFM, the change of plastic strain due to plastic deformation is assumed to cause the crack length extension. For a clear understanding of different mechanisms of rock fracturing under different cyclic loadings, a series of numerical analyses have been performed using ABAQUS FEM software. Inhomogeneity in this study is described with XFEM using Simpleware software, which makes it possible to implement the real failure surface geometry in tested rock samples including many inhomogeneity (flaws and micro–macro cracks) into the meshing stage of XFEM simulations. Then, XFEM works as usual by eliminating

the elements that reach the critical level. Once the element fails, it is deleted from the 3D solid. Therefore, degradation of rock stiffness occurs by deleting the local elements and this is not an inhomogeneous continuum. This method, implementing an inhomogeneous mesh structure into a FEM method, was created as a new and powerful technique to study many inhomogeneous continuums.

Schmidt (1980) suggested an approach called maximum normal stress (MNS) to evaluate fracture propagation and shape of the stress-induced main crack in FPZ. According to this approach, FPZ takes place because of the excessive tensile stresses around the tip of pre-existing cracks. For brittle material such as ceramic and rocks, nucleation and coalescence of microcracks are the main micromechanism of the damage. A numerical attempt has been done to investigate the distribution modes of principle stress at the vicinity of chevron notched cracks in CCNBD cyclic testing. It has been seen that the evolution of damage and stress distribution around the tip of pre-existing cracks in rocks were strongly found dependent on the loading history of given external stress during loading and unloading cycles. Figure 7 demonstrates the maximum tensile stress distribution and development of FPZ around the chevron notched crack in a CCNBD specimen under monotonic and cyclic loading. Figure 7 shows that the induced tensile stresses around the tip in the specimen tested under cyclic loading are lower than the induced tensile stresses in tested specimen under static loading. This means that the development of an FPZ and fracturing is possible with the lower ultimate loading than the expected values using cyclic loading. As seen in Fig. 7a, the high tensile stress concentration takes place just in front of the chevron crack. However, effective high tensile stress concentration takes place around the chevron crack beside the tip to develop an extensive FPZ zone under cyclic loading (Fig. 7b). Further, excessive distortion and dilatation can be seen in front of

Fig. 6 Different branching of the cracks in FPZ depending on the different amplitudes used with stepped cyclic loading: **a** 10 % UTS, **b** 50 % UTS and **c** 80 % UTS



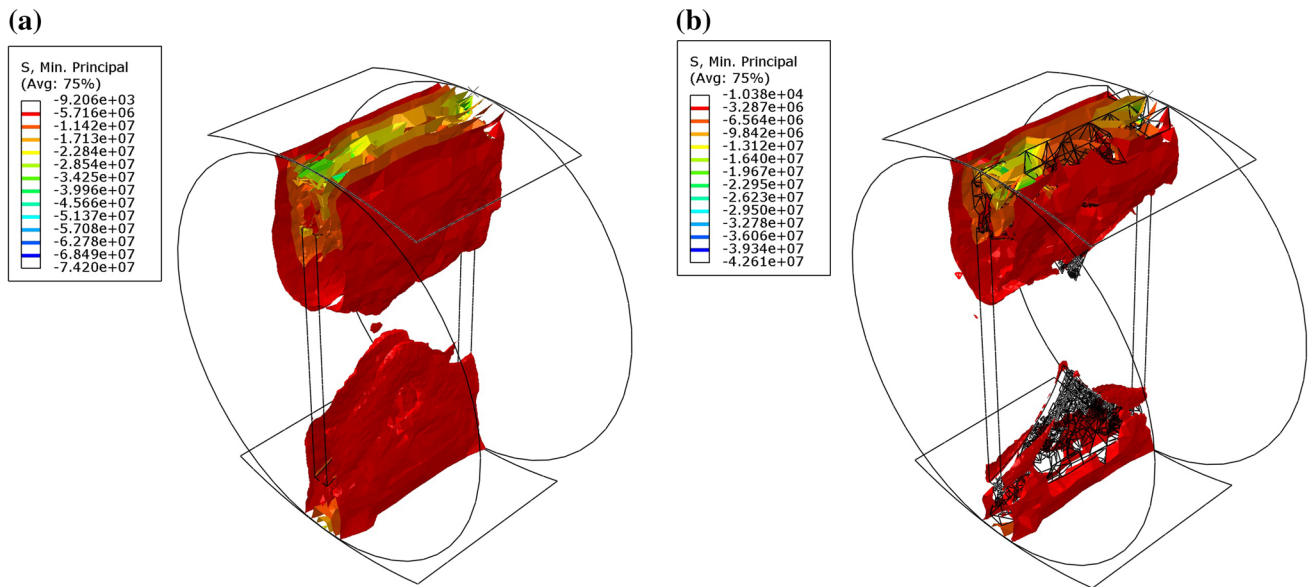


Fig. 7 Distribution of maximum tensile stress and development of FPZ around the tip of notched crack in a CCNBD specimen under the mode I, **a** static loading and **b** cyclic loading

chevron notch under the cyclic loading compared to the static loading (Fig. 7b).

With the further numerical analysis, the size of FPZ is obtained by substituting the obtained maximum tensile stresses into the Eqs. 4 and 5 as follows:

$$r_{FPZ}(\theta) \Big|_{\theta \neq 0} = \frac{1}{2\pi} \left(\frac{K_I}{\sigma_t} \right)^2 \cos^2 \left(1 + \left| \sin \frac{\theta}{2} \right| \right)^2 \quad (6)$$

The maximum expansion of FPZ can be calculated by derivation of the Eq. 6 above as:

$$\begin{aligned} \text{Max}(r_{FPZ})(\theta) \\ = \frac{1}{2} \frac{\left(2\cos\left(\frac{1}{2}x\right)^2 \sin\left(\frac{1}{2}x\right) + 3\cos\left(\frac{1}{2}x\right)^2 - 2\sin\left(\frac{1}{2}x\right) - 2 \right) \cos\left(\frac{1}{2}x\right) K_{IC}^2}{\sigma_t^2 \pi} \end{aligned} \quad (7)$$

Maximum dimension of FPZ can be achieved when the notch crack inclination angle becomes 60° ($\theta = 60^\circ$) where the maximum radius of FPZ obtained as:

$$\text{Max}(r_{FPZ}) = \frac{27}{32\pi} \frac{K_{IC}^2}{\sigma_t^2} \quad (8)$$

However, previous experimental and multi-variation analysis revealed that the maximum fracturing occurred in monsonite specimens when the $\theta = 45^\circ$ (Ghamgosar et al. 2014a). This numerical result is found quite helpful and close to the experimental results to determine the theoretical and real shape/size of FPZ in selected rock samples. Moreover, this result shows that the size of the FPZ model proposed by Schmidt (1980) is larger than the experimental results obtained with this study. Of course, there can be

many reasons to explain this difference between numerical and experimental results, such as effect of rock material properties, homogeneity and heterogeneity of rocks, grain size and matrix relationships.

5 Discussions

5.1 Static and Cyclic Loading Tests

The first test series comprised static tests conducted with the CCNBD specimens to understand the fracture propagation pattern and calculate the fracture toughness value of the tested rock discs under diametral monotonic compressive loading. One of the most interesting results is the fracturing difference between static and cyclic loading tests that the fractures propagate through the mineral and a typical brittle fracturing was seen on split surfaces of the failed rock specimens under static loading. However, a typical fatigue mechanism was observed by the accumulation of micro-fractures and plastic strain on fracture surface of the tested rock discs under cyclic loading. Crack mouth opening displacement (CMOD) was recorded simultaneously along x and y directions during both static and cyclic loading. All CMOD results showed that no plastic strain accumulation takes place until failure under static loading, whereas the diametral axial plastic strain was found increasing continuously under cyclic loading with a slow rate until failure.

It is shown with this research the crack propagation causing failure is possible with lower stress intensity values

(K_I) at the crack tip under cyclic loading than the critical stress intensity value (K_{IC}) found under static loading. This result goes against the classical theory, which predicts that there will be no crack growth as long as $K_{IC} > K_I$. In the classical fracture mechanics, cracks will propagate when the SIF, K , reaches or exceeds a critical SIF, K_C . In the engineering systems subjected to long-term loading, however, the classical fracture mechanics approach does not work, and crack growth can occur at a value of SIF that may be substantially lower than the critical value. This phenomenon is known as subcritical crack growth. The subcritical crack growth phenomenon was obtained clearly with the CCNBD fracturing tests with this research. Stress corrosion is the most common mechanism associated with subcritical crack growth in rock. However, it is certainly not the only mechanism by which subcritical crack growth occurs. Another mechanism that can be important, in certain circumstances, is fatigue crack growth. Stress corrosion and fatigue represent the major mechanisms of subcritical crack growth in rocks (Atkinson 1984; Costin and Holcomb 1981).

In general, fractures were found located on grain edges, especially around small grain minerals (<1.0 mm). However, some fractures were found propagated through the mineral grain in specimens with bigger size grains, but those transgranular fractures were stopped at the central portion of the rock sample due to some reasons.

The radius of the effective FPZ under static loading (FPZ_{Static}) was found around 1.3 mm, whereas this value was found minimum 2.5 mm for the cyclic loading tests. This indicates that FPZ obtained with the static loading is smaller than the FPZ obtained with the cyclic loading ($FPZ_{Static} < FPZ_{Cyclic}$). This finding can be verified with the obtained plastic strain accumulation shown in Figs. 8 and 9. Figures 8 and 9 show the stress–strain plots obtained under static and cyclic loading, respectively. Along the loading path to ultimate failure, pre-existing and stress-induced micro-flaws merge and coalescence into macro cracks leading to final failure. Those mechanisms cause ‘nonlinear behaviour’ in ‘stress–strain plots’ in rock mechanics. However, the linear section before the nonlinear part in stress–strain plots typically represents the elastic damage incurred in rock material under a mechanical loading. The nonlinear part in stress–strain plots obtained with the static loading is much smaller than the nonlinear damage obtained with cyclic loading. A comparison of the tensile stress distribution also reveals that maximum tensile stress for static loading was obtained 8 MPa, however, for cyclic loading was 3.5 MPa, and this shows 43 per cent reduction in tensile stress. Therefore, according to the tensile stress distribution, it can be claimed that $\sigma_{tStatic}^{FPZ} > \sigma_{tCyclic}^{FPZ}$ (see Figs. 8, 9). It should be noted that

FPZ, technically, is the area that tolerates partial loading until the stress component reaches the critical stage. The most appropriate model used FEM approaches; however, for the inhomogeneous material such as rock and concrete, FPZ dimension is dependent on the grain size, nature of loading and environmental conditions (Atkinson and Avdis 1980).

Development of an FPZ in front of a pre-existing crack in a material is the correspondence of the crack tip to the applied load. This phenomenon is proposed as ‘strain-softening and tension-softening’ by Hillerborg et al. (1976) and Horii and Nemat-Nasser (1985). Fracture energy is the energy that cracks need to develop and propagate in FPZ. Hillerborg et al. (1976) determined the required fracture energy for the brittle materials, such as rocks as the amount of energy absorbed by each new unit crack. Numerical analysis in this study showed that the calculated energy density in specimens was found different under the cyclic and static loadings since a sharp drop of energy density was found in FPZ, with the static loading modelling compared to the cyclic loading (Fig. 10). According to the results shown in Fig. 10, the required energy dissipation for the static loading is higher than the cyclic loading as the crack advances in front of notch crack in CCNBD specimen without any plastic strain as explained before. That is why the magnitude of required energy for the static loading is seven times higher than the cyclic loading. This achievement would be considered for the hard rock cutting area and other rock fragmentation methods by considering the effect of cyclic loading cause reduction on the required cutting energy. Strain energy density is the energy contained in unit weight of material that is used for crack propagation analysis in two- or three-dimensional and inhomogeneous problems. According to the Sih theory (1977), at the yield stage, total strain energy per unit volume absorbed by material equals the energy per unit volume stored in tensile loading.

Based on the numerical analysis results, the micro-fracture density in FPZ under cyclic loading is found higher than the obtained amount of micro-fractures under static loading, which are in good agreement with the laboratory results (Ghamgosar et al. 2014b) (Figs. 11, 12).

In conclusion, the rock fracturing in FPZ was investigated based on both laboratory and numerical analyses. Different numerical modellings were used to investigate the fracture propagation mechanism in FPZ under static and cyclic loading conditions separately. Laboratory observations showed that the micro-fracturing mechanism took place in rock matrix mostly due to the tension-softening under cyclic loading. Moreover, fatigue mechanism caused intragranular and intergranular fractures in FPZ, resulting in lower failure load under cyclic loading than the

Fig. 8 Tensile stress distribution and CMOD in front of the notch crack in CCNBD specimen tested under static loading

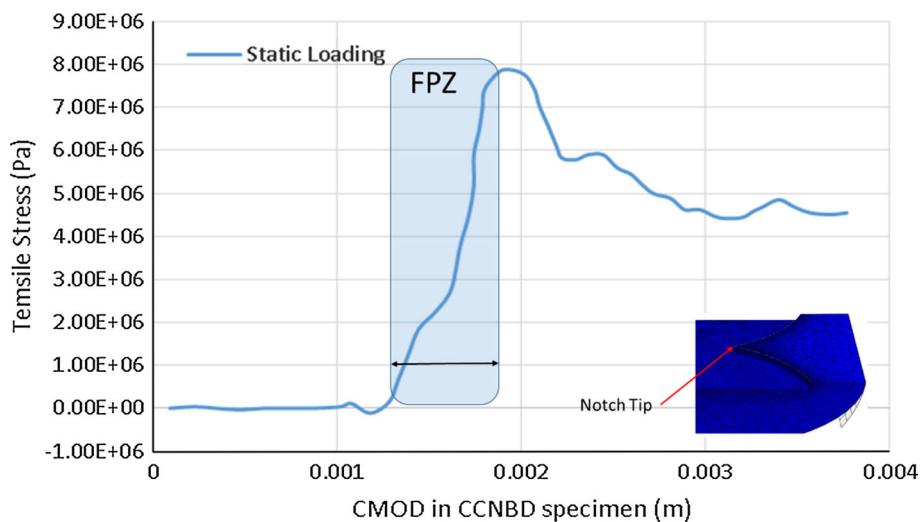


Fig. 9 Tensile stress distribution and CMOD in front of the notch crack in CCNBD specimen tested under cyclic loading

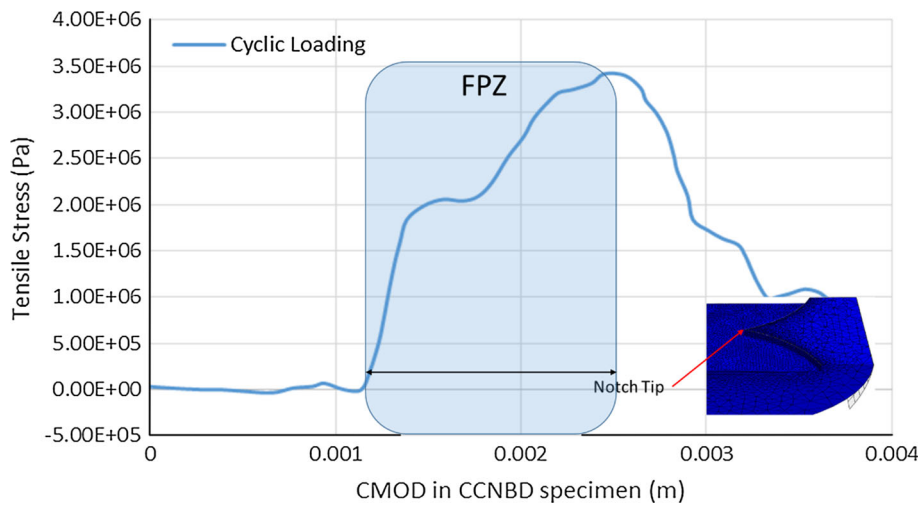
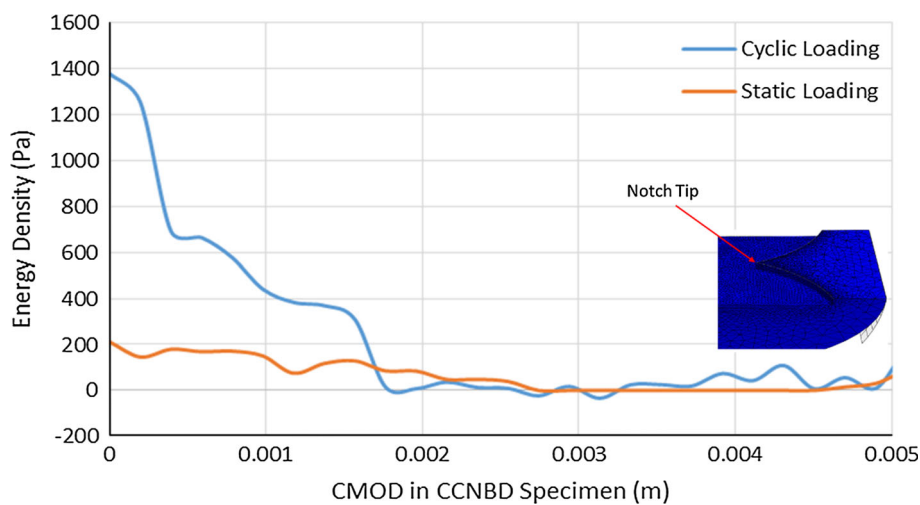


Fig. 10 Plastic strain energy in front of the notch crack in CCNBD specimen under the mode I fracture toughness cyclic and static loadings



obtained failure load under static loading. The fatigue mechanism, which is accumulation of plastic strain, helps to extend the FPZ by producing extreme amounts of microcracks whereas, by a macro-scale, sharp cleavage crack with the static loading. Concordantly, XFEM cyclic loading modelling results showed that the plastic strain components were found increasing due to the eliminated failed elements from the CCNBD solid model. Numerical modellings also showed that more displacement was obtained at the crack tip elements than the back of the

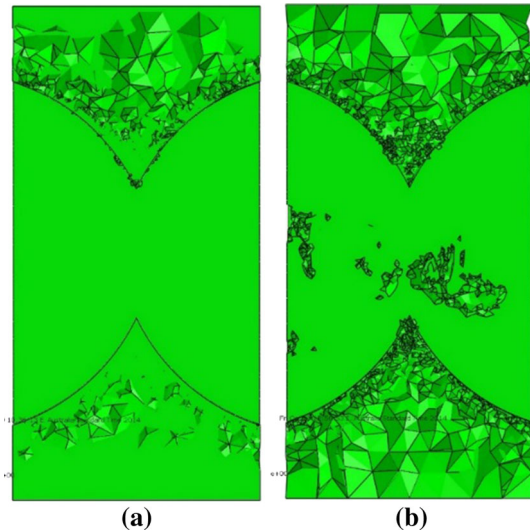


Fig. 11 Density of micro-fracture in front of the notch crack in a CCNBD specimen under, **a** static loading and **b** cyclic loading

Fig. 12 Failure pattern of CCNBD samples tested under, **a** static loading and **b** cyclic loading



crack tip. It means that the ‘crack bridging concept’ takes place at tip of the main crack in FPZ. However, it was expected that the FPZ started at the back of main crack tip causing larger FPZ under cyclic loading compared with the obtained FPZ under static loading.

5.2 Thin-Section Analysis

Some thin-section analyses were done on the failure surface of some CCNBD tested specimens (Figs. 13, 14). In general, fractures are located around grains, especially around small grains (<1.0 mm) with the stepped and continuous cyclic loading tests. Some micro-fractures were found propagated through the grain, but those transgranular fractures are stopped at the central portion of the rock sample due to some reasons. Different patterns of micro-fracture propagation are shown in Fig. 13. The obtained images showed that fatigue damage in specimens is strongly influenced by the failure of the matrix because of both intergranular fracturing and transgranular fracturing. The main characteristic is particle breakage under cyclic loading, which probably starts at contacts between particles and is accompanied by the production of very small fragments, probably resulting from frictional sliding within the weak matrix. Transgranular cracks may emanate from these regions, and intergranular cracks sometimes pass through the contact points. This stage can be correlated with a steady progression of damage and produces a general ‘loosening’ of the rock, which is a precursor to the formation of intergranular cracks (Fig. 13a). However,

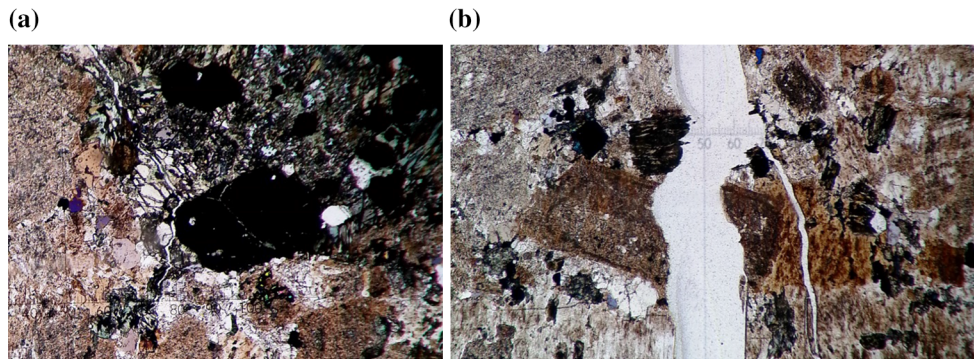


Fig. 13 Micro-fracture propagation through the monsonite matrix under, **a** cyclic loading and **b** through the grains under static loading

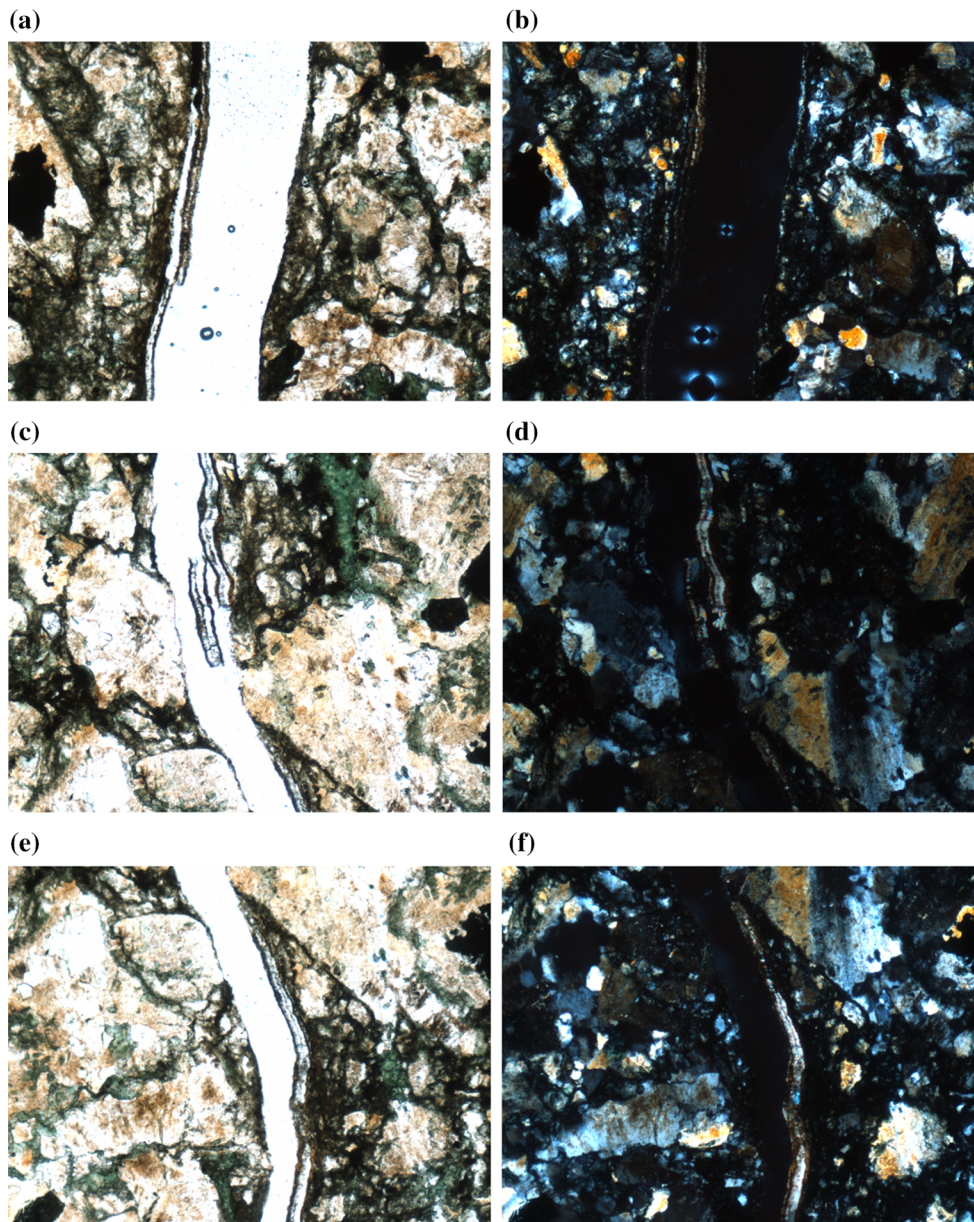


Fig. 14 Images of intergranular fracture. All images on the left (**a**, **c**, **e**) with uncrossed polarisers, while on the right (**b**, **d**, **f**), with crossed polarisers

intergranular cracks are formed due to particle breakage under static loading (Fig. 13b). This finding might explain why the ultimate fracture loading in cyclic loading is lower than the obtained value with the static loading.

This behaviour is explained with the grain–matrix relationship in some researches. For example, Fairhurst (1971) explains some micro-fractures stop growing into the matrix due to some other minerals in rock matrix because the strength of a mineral is almost a thousand times higher than a rock matrix. That is why some minerals behave as obstacles in front of a growing stress-induced crack.

Figures 14 and 15 illustrate intergranular and intragranular fractures in specimens tested under cyclic loading.

Based on the microscopic thin-section study results, the micro-fracturing and branching of subcritical fractures are found related with the FPZ zone and grain–matrix relationships. Moreover, the fracture propagation pattern is found dependent on the cyclic loading parameters such as amplitude and frequency. However, more micro-fractures and fatigue cracks were obtained with the stepped type cyclic loading than with the continuous type cyclic loading. This result shows that the amount of produced micro-

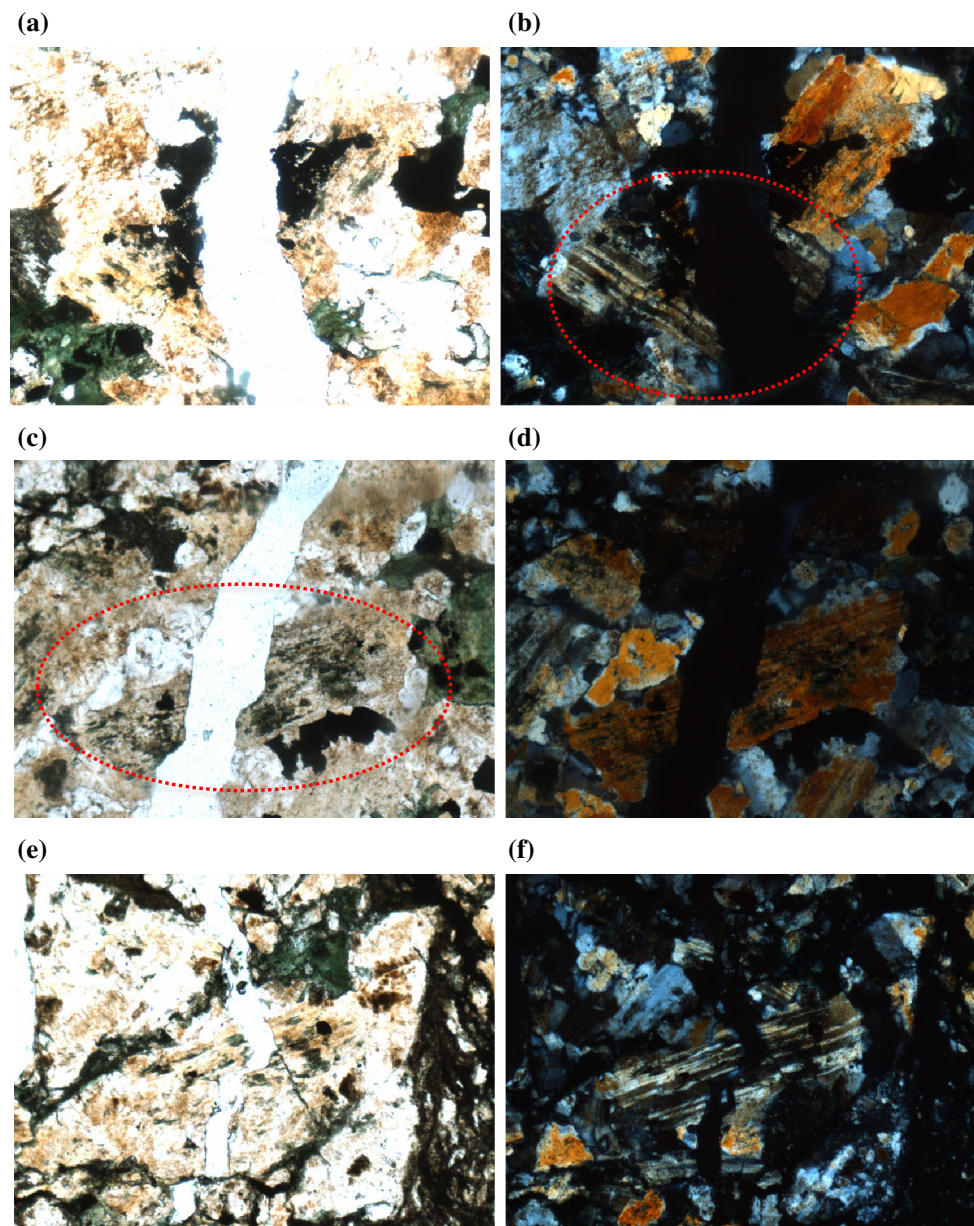


Fig. 15 Examples of fractures passing through minerals (transgranular fractures). A feldspar grain (Plagioclase) with a transgranular fracture, marked in red circle (a, b). An Augite (feldspar) clearly

shows a transgranular fracture (c, d). Finally, a transgranular fracture passing through several crystal grains of feldspar, quartz and amphibole (e, f)

fractures and plastic strain is dependent on the type of dynamic loading and related parameters.

6 Conclusions

This study was done to investigate and evaluate the micro-fracturing in FPZ developed in CCNBD specimens tested under cyclic and static loadings. The CT scan technique was successfully used to detect the propagation of micro-fractures and meso-fractures in FPZ. The following conclusions are drawn from this study:

1. The standard CCNBD tests were done with the Cadia Valley monsonite and Brisbane tuff samples under monotonic and cyclic loadings. Experimental and numerical modelling results showed that the size of FPZ developed under cyclic loading is greater than the developed FPZ under monotonic loading due to the fatigue damage mechanism leading to excessive micro-fractures and subcritical cracks.
2. The size of FPZ is found smaller than the size of FPZ obtained with LEFM models, such as the cohesive crack model. Moreover, the type of loading and unloading cycles is found significantly important for the unstable crack propagation around the crack tip. Numerical simulation results revealed that the length of FPZ developed under monotonic loading was 1.8 mm, whereas it was 2.5 mm under cyclic loading.
3. Numerical studies showed that the maximum principal stress (tensile stress) in FPZ developed under static loading is higher than the induced tensile stress under cyclic loading. The numerical stress analysis along the notched crack in CCNBD specimens showed a sharp drop of tensile stress value just after the yield point at the stress–strain plot of monotonic loading. However, a gradual stress drop after the yield point was noted at the stress–strain plot of cyclic loading.
4. Numerical simulations showed that the maximum size of FPZ takes place when $\theta = 60^\circ$. However, laboratory experiments and multi-variation analysis showed that the maximum FPZ was obtained when $\theta = 45^\circ$.
5. CT scan observations show that the propagation of subcritical crack and development of excessive micro-fracturing are found increasing with the increasing amplitude and frequency of the cyclic loading.
6. To investigate possible differences between static and fatigue failure, the fracture surfaces of monotonically and cyclically tested CCNBD specimens were also observed by using thin-section analyses. When compared with static rupture, the main differences are twofold: (1) the number of fragments produced is much greater under cyclic loading than under static

loading, and (2) intergranular cracks are formed due to particle breakage under cyclic loading compared with smooth and bright cracks along cleavage planes under static loading. Obviously, the macro-scale main crack causing failure is seen in cement without any dust or debris material under monotonic loading. Typical sparkling cleavage cracks resulted when the rupture of the crystals occurred along cleavage planes.

Acknowledgments Newcrest Mining is acknowledged for funding the Scholarship of the first author during the course of the research on which this paper was in part based, and for providing monsonite core samples from Cadia Valley, which were used for testing purposes. Golders Associates are acknowledged for providing access to Brisbane tuff core samples from the CLEM7 tunnel project in Brisbane, which were used for testing purposes. The author would like to express his sincere thanks to Professor Arcady Dyskin and Professor Eduardo A. G. Marquesn for their kind help and technical advice.

References

- Anderson TL (2005) Fracture mechanics: fundamentals and applications, CRC press
- Atkinson BK (1984) Subcritical crack growth in geological materials. *J Geophys Res Solid Earth* (1978–2012) 89:4077–4114
- Atkinson BK, Avdis V (1980) Fracture mechanics parameters of some rock-forming minerals determined using an indentation technique. *Int J Rock Mech Min Sci* 17:383–386
- Costin L, Holcomb D (1981) Time-dependent failure of rock under cyclic loading. *Tectonophysics* 79:279–296
- Eberhardt E, Stead D, Stimpson B, Read R (1998) Identifying crack initiation and propagation thresholds in brittle rock. *Can Geotech J* 35:222–233
- Erarslan N, Williams D (2012) Mechanism of rock fatigue damage in terms of fracturing modes. *Int J Fatigue* 43:76–89
- Evans A (1972) A method for evaluating the time-dependent failure characteristics of brittle materials—and its application to polycrystalline alumina. *J Mater Sci* 7:1137–1146
- Evans A (1974) Slow crack growth in brittle materials under dynamic loading conditions. *Int J Fract* 10:251–259
- Evans A, Fuller E (1974) Crack propagation in ceramic materials under cyclic loading conditions. *Metall Trans* 5:27–33
- Fairhurst C (1971) Fundamental considerations relating to the strength of rock. In: Colloquium on rock fracture, Ruhr University, Bochum, Germany, Veröff. Inst. Bodenmechanik und Felsmechanik (Karlsruhe), vol 55, pp 1–56
- Fowell R, Xu C (1994) The use of the cracked Brazilian disc geometry for rock fracture investigations. *International Journal of Rock Mechanics and Mining Sciences & Geomechanics Abstracts*. Elsevier, pp 571–579
- Fowell RJ, Hudson JA, Xu C, Chen JF, Zhao X (1995) Suggested method for determining mode I fracture toughness using cracked chevron notched Brazilian disc (CCNBD) specimens. *Int J Rock Mech Min Sci Geomech Abstr* 32(1):57–64
- Franklin JA, Zongqi S, Atkinson BK, Meredith PC, Rummel F, Mueller W, Nishimatsu Y, Takahashi H, Costin LS, Ingraffea AR, Bobrov GF (1988) Suggested methods for determining the fracture toughness of rock. *Int J Rock Mech Min Sci Geomech Abstr* 25:71–96
- Ghamgosar M, Erarslan N, Williams D (2014) Assessment of rock mechanics parameters for improved waste disposal management

- and containment. The 7th International Congress on Environmental Geotechnics Melbourne
- Ghamgosar M, Erarslan N, Williams D (2014) In Press. Multiple factorial analysis of rock fragmentation under various cyclic loading conditions. *ISRM 13th International Congress on Rock Mechanics*
- Giner E, Sukumar N, Taracón JE, Fuenmayor FJ (2009) An Abaqus implementation of the extended finite element method. *Eng Fract Mech* 76:347–368
- Griffith A (1920) VI The Phenomena of rupture and flow in solids. *Phil Trans Roy Soc (Lon) A* 221:163–198
- Gross D, Seelig T (2011) *Fracture mechanics: with an introduction to micromechanics*. Springer
- Hillerborg A, Modéer M, Petersson PE (1976) Analysis of crack formation and crack growth in concrete by means of fracture mechanics and finite elements. *Cem Concr Res* 6:773–781
- Horii H, Nemat-Nasser S (1985) Compression-induced microcrack growth in brittle solids: axial splitting and shear failure. *J Geophys Res Solid Earth* (1978–2012) 90:3105–3125
- Horii H, Nemat-Nasser S (1986) Brittle failure in compression: splitting, faulting and brittle-ductile transition. *Philosophical Transactions for the Royal Society of London. Series A, Mathematical and Physical Sciences*, pp 337–374
- Labuz J, Shah S, Dowding C (1987) The fracture process zone in granite: evidence and effect. *International Journal of Rock Mechanics and Mining Sciences & Geomechanics Abstracts*. Elsevier, pp 235–246
- Maji A, Wang J (1992) Experimental study of fracture processes in rock. *Rock Mech Rock Eng* 25:25–47
- Mindess S (1984) The effect of specimen size on the fracture energy of concrete. *Cem Concr Res* 14:431–436
- Ouchterlony F (1980) Review of fracture toughness testing of rock. *SveDeFo, Stiftelsen Svensk Detonikforskning*, pp 145–159
- Schmidt RA (1980) A microcrack model and its significance to hydraulic fracturing and fracture toughness testing. *The 21st US Symposium on Rock Mechanics (USRMS)*. American Rock Mechanics Association
- Schmidt R, Lutz T (1979) K_{Ic} and J_{Ic} of Westerly granite—effects of thickness and in-plane dimensions. *Fract Mech Appl Brittle Mater ASTM STP* 678:166–182
- Sih GC (1977) *Mechanics of Fracture: elastodynamic crack problems*, vol 4. Noordhoff International Publishing, Leyden, pp 50–60
- Spyropoulos C, Griffith WJ, Scholz CH, Shaw BE (1999) Experimental evidence for different strain regimes of crack populations in a clay model. *Geophys Res Lett* 26:1081–1084
- Tang C-A, Yang Y-F (2012) Crack branching mechanism of rock-like quasi-brittle materials under dynamic stress. *J Cent South Univ* 19:3273–3284
- Wang QZ, Jia XM, Kou SQ, Zhang ZX, Lindqvist PA (2004) The flattened Brazilian disc specimen used for testing elastic modulus, tensile strength and fracture toughness of brittle rocks; analytical and numerical results. *Int J Rock Mech Min Sci* (1997) 41:245–253
- Whittaker BN, Singh RN, Sun G (1992) *Rock fracture mechanics: principles, design, and applications*, vol 71. Elsevier, Amsterdam, New York, pp 81–110